Langmuir

ARTICLE

pubs.acs.org/Langmuir

Theory and Simulation of Angular Hysteresis on Planar Surfaces

M. J. Santos[†] and J. A. White[*,†,‡]

[†]Departamento de Física Aplicada, Universidad de Salamanca, 37008 Salamanca, Spain

ABSTRACT: A simple model is proposed to simulate contact angle hysteresis in drops on a planar surface. The model is based on assuming a friction force acting on the triple contact line in such a way that the contact line keeps fixed for contact angles comprised between the advancing angle and the receding one and is allowed to move in order to avoid angles outside this interval. The model is straightforwardly applied to axisymmetric drops for which a simple solution of the Young−Laplace equation can be obtained. A variation of the method has also been implemented for nonaxisymmetric drops by resorting to the public-domain "Surface Evolver" software. Comparison with experiments shows the excellent performance of the model.

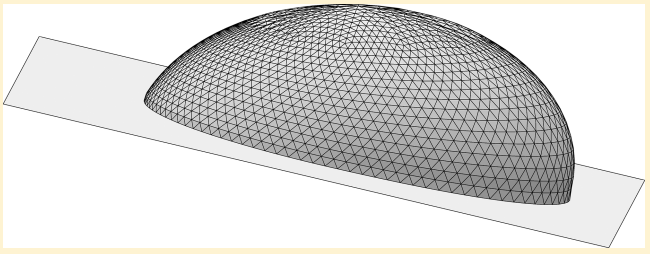

INTRODUCTION

Understanding the shape of a liquid drop in mechanical equilibrium on a planar surface is an important issue in both surface science and in many engineering applications. A key aspect in determining this shape is the analysis of the contact angle of the liquid drop with the surface. It is well-known that this contact angle can be obtained from a balance between the liquid−vapor surface tension, σ_{lv}, the solid−vapor surface tension, σ_{sv}, and the liquid−solid surface tension, σ_{ls}. This balance of surface forces is given by Young's equation,[1]

$$\sigma_{sv} - \sigma_{ls} = \sigma_{lv}\cos\theta_Y \quad (1)$$

where θ_Y is the contact angle coming from the Young equation. This equation holds for ideal systems in which the solid surface is smooth, homogeneous, and rigid so that there is only one equilibrium state characterized by a single contact angle θ_Y.

The situation is quite different in real systems because nearly all solid surfaces are rough and chemically heterogeneous to some extent. This implies that θ_Y is in general not equal to the apparent contact angle[2] measured in an experiment. Consequently, a direct application of Young's eq 1 is no longer valid in real systems and one must resort to modifications like the Cassie equation for chemically heterogeneous substrates,[3] or the Wenzel[4] and the Cassie and Baxter[5] equations for rough substrates. In addition, due to roughness and chemical heterogeneity, most real systems exhibit contact angle hysteresis in which there is a range of practically stable apparent contact angles comprised between its lower limit, the receding contact angle θ_{rec}, and its upper limit given by the advancing contact angle θ_{adv}.

Several attempts have been made in the past to study drops with contact angle hysteresis in a semiempirical way, without entering into the details of its microscopic origin. In this context, the pioneering work by Adam and Jessop[6] included an external force in Young's eq 1 so that one has the following:

$$\sigma_{sv} - \sigma_{ls} = \sigma_{lv}\cos\theta_{adv} + f \quad (2)$$

for an advancing situation, and,

$$\sigma_{sv} - \sigma_{ls} = \sigma_{lv}\cos\theta_{rec} - f \quad (3)$$

for a receding situation. In eqs 2 and 3, f is a friction force per unit length, acting on the triple contact line with equal intensity for advancing and receding angles. We note that a different interpretation for f was given later by Good.[7] Some early works[8−10] studied contact angle hysteresis for drops on inclined plates by considering a fixed circular contact line as an approximation valid for small drops or low inclinations (note that a static friction force is implicitly assumed when one considers a fixed contact line). Dussan and Chow[11,12] also studied drops on inclined plates but assuming elongated drops with a contact line formed by two semicircular arcs joined by with two parallel sides along the direction of inclination. A finite-elements simulation scheme in which the contact line is allowed to move was proposed by Iliev[13,14] by considering a retention term proportional to the area swept by the virtual motion of the contact line. An optimization-problem approach was addressed by Dimitrakopoulos and Higdon[15] by searching over all contact lines with local contact angles θ_n such that $\theta_{rec} \le \theta_n \le \theta_{adv}$.

In the spirit of the above-mentioned works, the goal of the present work is to propose a new approach to static contact angle hysteresis assuming an empirical friction force per unit of contact line length so that the contact line keeps fixed for any angle in the range $\theta_{rec} < \theta < \theta_{adv}$ and moves in order to prevent angles outside this range. In this context, we would like to note that from a microscopic viewpoint one can assume that the friction force is due to the pinning forces exerted by defects on the contact line as argued by Joanny and de Gennes.[16,17]

This work is structured as follows. We first consider an approach to the problem which is only valid for axisymmetric

Received: July 19, 2011
Revised: October 6, 2011
Published: November 03, 2011

drops and is based on the solution of the Young−Laplace equation in cylindrical coordinates. Then we resort to the well-known public-domain "Surface Evolver" software[18] incorporating a friction force in the search of the stable shape of the liquid drop. This approach, which is also valid for nonaxisymmetric drops, has allowed us to design a new method for measuring contact angles in the Surface Evolver. Next, we compare the results of these approaches with experimental data. Finally, we apply the new Surface-Evolver approach to the nonaxisymmetric situation of a liquid drop on an inclined surface. We conclude with a brief summary of this work.

SIMPLE APPROACH FOR AXISYMMETRIC DROPS

The Young−Laplace equation[1,19] states that the pressure difference Δp across a fluid interface at equilibrium is proportional to the surface tension σ_{lv} and the mean curvature $\mathcal{H} = (1/R_1 + 1/R_2)/2$ where R_1 and R_2 are the principal radii of curvature. Under gravity one has the following:

$$\Delta p = \sigma_{lv}\left(\frac{1}{R_1} + \frac{1}{R_2}\right) - \Delta\rho g z \tag{4}$$

where $\Delta\rho g z$ is an hydrostatic pressure term in which $\Delta\rho$ represents the difference in density of liquid and vapor phases, g is the acceleration due to gravity, and z is the height.

In general, the Young−Laplace equation is a nonlinear partial differential equation difficult to handle but, for cylindrical symmetry, it becomes a system of ordinary differential equations which can be expressed in terms of the arc length s of the drop profile (see eq 1 of ref 20). We note that this system of ordinary differential equations is the starting point of Axisymmetric Drop Shape Analysis (ADSA).[20]

The solution of the axisymmetric Young−Laplace equations for a sessile drop allows one to obtain the tangential angle of the drop profile $\theta(s,b,c)$, the axial coordinate $z(s,b,c)$, the radial coordinate $R(s,b,c)$, the area of the interface liquid−vapor $A(s,b,c)$, and the volume $V(s,b,c)$ as a function of the arc length s, the curvature at the apex of the drop $b = 1/r_0$, where r_0 is the curvature radius at the apex, and the capillary constant $c = 1/l_0^2 = \Delta\rho g/\sigma_{lv}$ where l_0 is the capillary length.

If the volume V and the contact angle θ of a liquid drop with capillary constant c are known, then one can obtain the apex curvature b and the arc length at the triple contact line s_c from solving the system of equations:

$$V(s_c,b,c) = V;\theta(s_c,b,c) = \theta \tag{5}$$

Other quantities of interest are then readily obtained: for instance, the height of the drop comes from $H = z(s_c,b,c)$ and the radius of the triple contact line is given by $R = R(s_c,b,c)$. Conversely, if the drop is known to have a volume V and a contact line radius R one must solve:

$$V(s_c,b,c) = V;R(s_c,b,c) = R \tag{6}$$

to obtain b and s_c from which the contact angle θ can be calculated. We note that this is somehow different from the ADSA-D method in which the maximum diameter D is considered.[20]

Next we consider a dynamic one-cycle contact angle (DOCA)[21] measurement of the advancing and receding contact angles of a sessile drop. A liquid drop with initial volume V_{ini} is deposited in a flat horizontal surface. We assume that the drop has a initial contact angle θ_{ini} in the range $\theta_{rec} \le \theta_{ini} \le \theta_{adv}$. The drop volume is slowly increased at constant rate until it reaches a final volume V_{fin} and then decreased at the same rate to the initial volume V_{ini}. During the growing process one observes that the triple contact line keep fixed (R = constant) until the advancing contact angle θ_{adv} is reached and then the contact line moves (R grows) while $\theta = \theta_{adv}$ = constant until the growing is stopped ($V = V_{fin}$). In the initial stage of the shrinking process, the contact line keeps fixed while the contact angle decreases until it reaches its receding value and the triple contact line radius starts to decrease. We note that most liquid−solid systems give rise to time-dependent receding contact angles[21] but these situations are ascribed to changes in the solid (surface swelling and adsorption) and, although an appropriate microscopic description is out of the scope of this work, in the Results Section, we will give a semiphenomenological approach to such systems. Constant receding contact angles have been observed in some biodegradable surface-liquid systems, such as water on poly(lactic acid)-coated silicon surfaces.[21,22]

The description of a DOCA experiment with eqs 5 and 6 is straightforward:

1. *Initial drop*: The initial volume V_{ini} and the initial contact angle θ_{ini} are known. Using eq 5, one determines b and s_c from which the initial radius R_{ini} is obtained.
2. *Growing drop with* $\theta < \theta_{adv}$: In this situation, the volume $V > V_{ini}$ and the radius $R = R_{ini}$ are known. Using eq 6, one determines b and s_c from which the contact angle is obtained. When θ becomes θ_{adv}, the system goes to an advancing situation.
3. *Advancing situation*: The volume V and the contact angle $\theta = \theta_{adv}$ are known. The contact line radius R is calculated using eq 5. When $V = V_{fin}$ the maximum radius R_{max} is obtained.
4. *Shrinking drop with* $\theta > \theta_{rec}$: In this situation, the volume $V < V_{fin}$ and the radius $R = R_{max}$ are known. Using eq 6, one determines the contact angle. When θ becomes θ_{rec} the system goes to a receding situation.
5. *Receding situation*: The volume V and the contact angle $\theta = \theta_{rec}$ are known. The contact line radius R is calculated using eq 5. When $V = V_{ini}$ the calculations stop.

The question then arises as to how to reexpress this simple picture of a DOCA experiment in terms of a friction force acting on the contact line. The answer to this question is straightforward by considering an approach similar to that of eqs 2 and 3 but with different values of the friction force per unit length f depending on the situation. One has the following:

$$\sigma_{sv} - \sigma_{ls} = \sigma_{lv}\cos\theta_{adv} + f_{adv} \tag{7}$$

for an advancing axisymmetric drop, and the following:

$$\sigma_{sv} - \sigma_{ls} = \sigma_{lv}\cos\theta_{rec} - f_{rec} \tag{8}$$

for a receding axisymmetric drop. Comparing eqs 7 and 8 with eq 1 we obtain,

$$f_{adv} = \sigma_{lv}(\cos\theta_Y - \cos\theta_{adv}) \tag{9}$$

and

$$f_{rec} = \sigma_{lv}(\cos\theta_{rec} - \cos\theta_Y) \tag{10}$$

We note that the usual assumption,

$$\theta_Y = \frac{\theta_{rec} + \theta_{adv}}{2} \tag{11}$$

for the Young contact angle leads to $f_{rec} \neq f_{adv}$. Imposing $f_{rec} = f_{adv}$ like in eqs 2 and 3 gives rise to a slightly different but also usual assumption for the Young contact angle:

$$\theta_Y = \arccos\left(\frac{\cos\theta_{rec} + \cos\theta_{adv}}{2}\right) \quad (12)$$

Another prescription for the Young contact angle of a sessile drop has been given by Tadmor[23] by taking into account the line energy associated with the triple contact line.

A static friction force per unit length f_θ is acting when the contact line is fixed. In this case θ belongs to the interval $\theta_{rec} < \theta < \theta_{adv}$, and

$$\sigma_{sv} - \sigma_{ls} = \sigma_{lv}\cos\theta - f_\theta \quad (13)$$

with

$$f_\theta = \sigma_{lv}(\cos\theta - \cos\theta_Y) \text{ if } \theta_{rec} < \theta < \theta_{adv} \quad (14)$$

Figure 1 shows a contact angle hysteresis cycle using the above algorithm. In Figure 1a the contact angles are plotted as a function of the volume while in Figure 1b we represent the contact line radius. Figure 1c shows the dimensionless friction force f_θ/σ_{lv} as a function of the volume. The maximum value of f_θ is f_{rec}, while its minimum value is $-f_{adv}$. We note that negative values of f_θ simply indicate that the friction force is directed toward the center of the triple-line circumference, opposing the advancing direction. Analogously, positive values of f_θ indicate that the friction force is directed outward the center of the triple-line circumference, now opposing the receding direction.

In Figure 1 we have considered an initial volume V_{ini} = 0.030 cm^3 and a final volume V_{fin} = 0.118 cm^3 of water deposited on a poly(lactic acid)-coated silicon surface for which θ_{adv} = (79.82 ± 0.28)° and θ_{rec} = (60.97 ± 0.31)°.[22] The capillary length of water is l_0 = 2.72 mm and the Young contact angle is assumed to take the value $\theta_Y = (\theta_{rec} + \theta_{adv})/2$ = 70.40°. For simplicity we also consider that the initial contact angle θ_{ini} is equal to θ_Y. We note that in order to obtain the results presented in Figure 1 we have increased the volume from V_{ini} to V_{fin} at constant rate and then we have decreased it again to V_{ini}.

To conclude, the simple approach presented in this Section is only valid for axisymmetric drops for which the cylindrical symmetry plays an essential role. For nonaxisymmetric drops the Young−Laplace equation cannot be reexpressed as a set of system of ordinary differential equations. Furthermore, instead of having a single contact angle, θ, in general the system has contact angles that depend on the position. In the forthcoming Section, we will deal with nonaxisymmetric drops for which a solution of the Young−Laplace equation can be obtained by resorting to a finite-elements treatment like the one provided by the 'Surface Evolver' software.[18] Nonetheless, this finite-elements approach of wider applicability will be based on the ideas presented in this Section.

"SURFACE EVOLVER" IMPLEMENTATION

The energy of a sessile drop can be expressed as follows:

$$U = U_S + U_g \quad (15)$$

where U_g is the gravity contribution,

$$U_g = -\iiint_V \Delta\rho\mathbf{g}\cdot\mathbf{r}\,dV \quad (16)$$

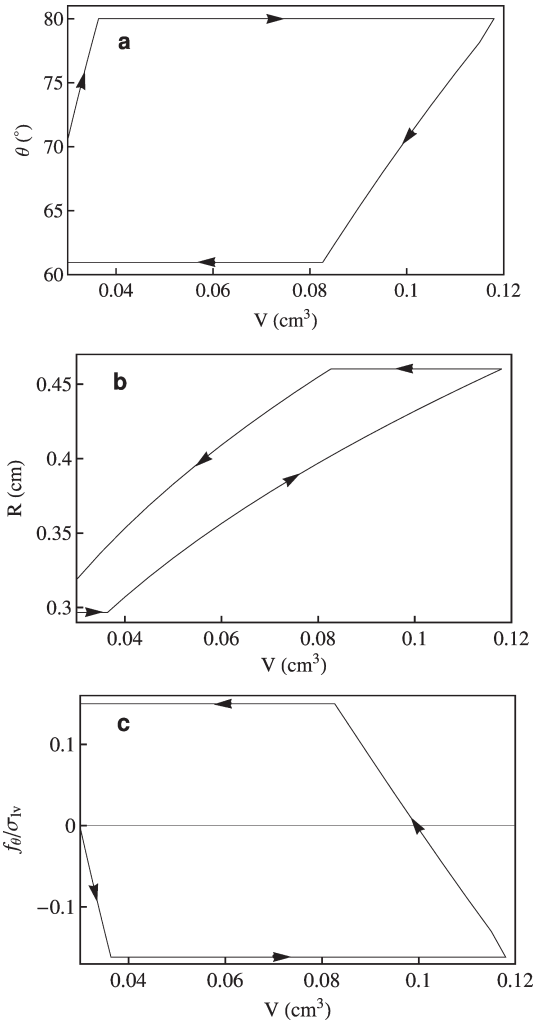

Figure 1. Contact angle hysteresis cycle for a drop of water on a poly(lactic acid)-coated silicon surface. (a) Contact angle θ vs volume, V. (b) Contact line radius, R, vs volume. (c) Friction dimensionless force f_θ/σ_{lv} vs volume. The arrows indicate the direction of volume change.

being $\mathbf{g}$ the gravity acceleration vector, and U_S is a surface contribution:

$$U_S = \iint_{A_{ls}} \sigma_{ls}\,dA + \iint_{A_{lv}} \sigma_{lv}\,dA + \iint_{A_{sv}} \sigma_{sv}\,dA \quad (17)$$

where A_{ls} is the area of the drop in contact with the surface, A_{lv} is the area of the liquid−vapor interface, and A_{sv} is the surface free-area. Using Young's eq 1 this surface contribution becomes:[24−27]

$$U_S = \sigma_{lv}A_{lv} - \iint_{A_{ls}} \sigma_{lv}\cos\theta_Y\,dA + U_{S0} \quad (18)$$

where U_{S0} is a constant contribution.

A variational approach can be considered by minimizing functionals 15−18 with respect to drop shape and subjected to the constraint of constant drop volume. In this case, it can be shown that the Young−Laplace equation is the Euler−Lagrange equation of the variational principle. Therefore, both the partial differential equation approach of the Young−Laplace equation and the integral approach provided by the variational principle are equivalent and yield the equilibrium shape of the drop.

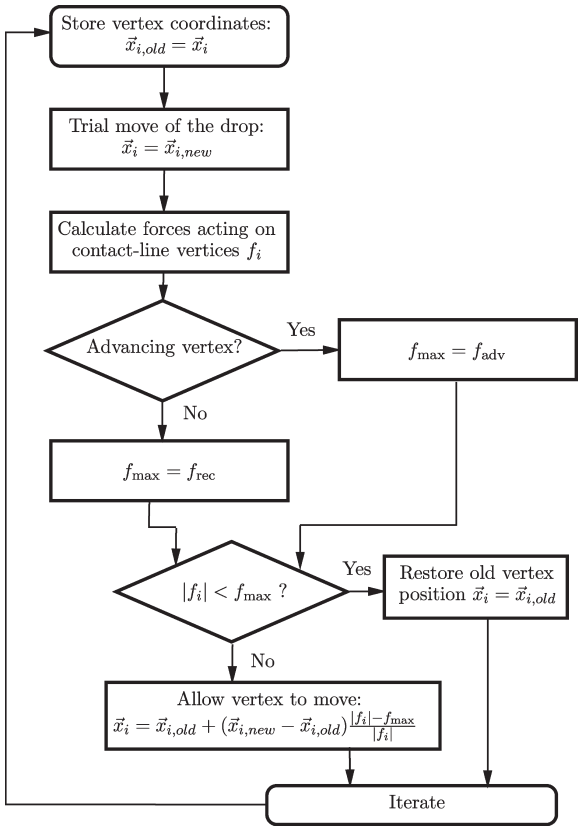

Figure 2. Flowchart of the algorithm used in the Surface Evolver.

As is well-known, the "Surface Evolver" software by Brakke[18] provides an appropriate means of solving the above variational problem since it is especially designed for finding the minimal surface subjected to a set of constraints. The Surface Evolver uses a finite-element method in which the surface is represented by a triangular tessellation in which the building blocks are vertices, edges, and facets. Several works can be found in the literature showing the use of the Surface Evolver in the field of fluid interfacial phenomena.[24−36]

Brandon et al.[24] have shown how the Surface Evolver can give rise to contact angle hysteresis for a chemically heterogeneous planar surface. This software has been also used for microstructured surfaces that also lead to contact angle hysteresis.[25,33−36] In these cases, the system has a well-defined energy functional and the constrained minimization process of the Surface Evolver is also well-defined. However, the simple model presented in the preceding Section cannot be directly implemented in this software because it considers an empirical friction force which leads to dissipation and the energy of the system is not conserved which preclude a proper energy minimization.

Here, we propose a method for implementing an empirical friction force in the Surface Evolver by adding local constraints in the *evolution* of the system toward a stable configuration. The idea is extremely simple: By resorting to a virtual displacement of the drop, the modulus of the force per unit length $|f_i|$ acting on each vertex of the contact line is measured and compared with the maximum friction force ($f_{max} = f_{adv}$ if the vertex is *advancing* and $f_{max} = f_{rec}$ if the vertex is *receding*). If the measured force is less than the maximum friction force the vertex is kept fixed. If this force is larger than the maximum friction force, then the vertex is allowed to move. In the latter case, the displacement of the vertex is scaled by the ratio $(|f_i| - f_{max})/|f_i|$ in order to account for the friction. We note that the vertex motion in the Surface Evolver is proportional to the force acting on the vertex divided by σ_{lv}. This provides a direct way of measuring the force and justifies the scaling of the vertex displacement for $|f_i| > f_{max}$. Figure 2 shows a flowchart of the algorithm used to introduce a friction term in the Surface Evolver. This algorithm should be used instead of the usual g command of the Surface Evolver. Denoting gfric the compound command that implements the algorithm of Figure 2, after initialization one only has to iterate this command in order to obtain an stable drop shape for a given drop volume, i.e., gfric 1000. We note that the only input required are the advancing and receding contact angles as well as a given prescription for the Young contact angle, e.g., eq 11 or eq 12.

Contact Angle Measurement. The usual way of measuring contact angles in the Surface Evolver is by a direct calculation of the angles between the substrate and the triangular facets that have an edge in the triple line. This direct approach is very easy to implement and yields fairly good results. As we will see below, this direct measurement has the important drawback that it is severely affected by mesh-size effects so that one need to consider a large number of vertices in the triangular tessellation of the drop in order to obtain reliable results.

Since the algorithm of Figure 2 is based on the measurement of the forces f_i acting on the vertices of the triple-line here we propose an alternative method for contact angle measurement which makes use of the relations between forces and contact angles that have been derived in the preceding Section. More concretely, from eq 14, for a receding situation one has,

$$\theta_i = \begin{cases} \theta_{rec} & \text{if } |f_i| \geq f_{rec}, \\ \arccos(\cos\theta_Y + |f_i|/\sigma_{lv}) & \text{if } |f_i| < f_{rec}, \end{cases} \quad (19)$$

where f_{rec} is given by eq 10. For an advancing situation one has,

$$\theta_i = \begin{cases} \theta_{adv} & \text{if } |f_i| \geq f_{adv}, \\ \arccos(\cos\theta_Y - |f_i|/\sigma_{lv}) & \text{if } |f_i| < f_{adv}, \end{cases} \quad (20)$$

where f_{adv} is given by eq 9. In eqs 19 and 20, the notation θ_i indicates that this is the contact angle obtained from the force F_i measured at vertex i. The force per unit length f_i is readily obtained from

$$f_i = \frac{2F_i}{l_{i,1} + l_{i,2}} \quad (21)$$

where $l_{i,1}$ and $l_{i,2}$ are the lengths of the two edges attached to vertex i that belong to the triple line. As a matter of fact, using virtual displacements in the Surface Evolver, one directly obtains $|F_i|/\sigma_{lv}$ and therefore, from eqs 21 and 19 or 20, one obtains the contact angle θ_i. For axisymmetric drops, it is advisable to perform a contact angle average along the triple line. Following Brandon et al.[24] we shall consider the following expression for the average contact angle $\bar{\theta}$.

$$\bar{\theta} = \frac{\oint_C \theta \mathrm{d}l}{\oint_C \mathrm{d}l} \quad (22)$$

where the line integrals are performed along the closed path C defined by the triple line and θ is the local contact angle measured along C. In our case, eq 22 reduces to the

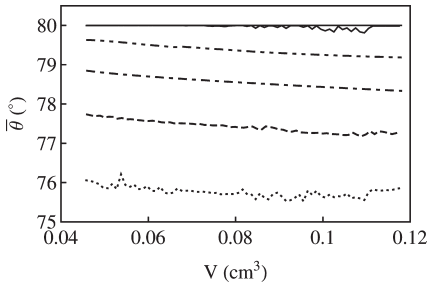

Figure 3. Average contact angle for a drop of water on a poly(lactic acid)-coated silicon surface vs volume in an advancing situation. Solid lines: results of the new method based on the measurement of forces. Other lines: results of the direct measurement of the contact angles N = 24 (dotted line), N = 48 (dashed line), N = 96 (dot-dashed line), and N = 192 (dot-dot-dashed line).

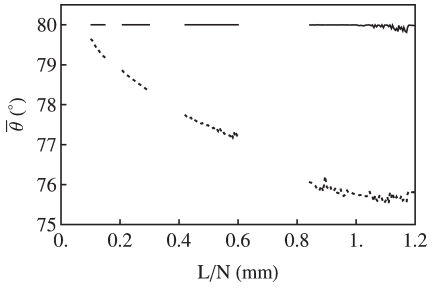

Figure 4. Average contact angle for a drop of water on a poly(lactic acid)-coated silicon surface vs the mean edge length in the triple line L/N. Solid lines: results of the new method based on the measurement of forces. Dotted lines: results of the direct measurement of the contact angles.

following:

$$\overline{\theta} \approx \frac{\sum_{i=1}^{N} \theta_i (l_{i,1} + l_{i,2})}{\sum_{i=1}^{N} (l_{i,1} + l_{i,2})} \tag{23}$$

where N is the number of vertices in the triple line. We note that the triple line length L is simply,

$$L = \oint_C \mathrm{d}l \approx \frac{1}{2} \sum_{i=1}^{N} (l_{i,1} + l_{i,2}) \tag{24}$$

In order to test the performance of the new method of measuring contact angles we have considered the same system as that of Figure 1 in an advancing situation in which the drop volume increases from V = 0.046 cm^3 to V = 0.118 cm^3. In Figure 3, we present the results of the average contact angle $\overline{\theta}$ measured with both the direct and the new method for different values of the number of vertices in the triple line, N = 24, 48, 96, and 192, which correspond to a total number of vertices of N_v = 133, 505, 1969, and 7777, respectively. We have not considered larger meshes due to the exponentially increasing computational cost. As one can observe the new method yields very good results for $N \geq 48$, showing some noise for N = 24. The direct measurement method is subjected to mesh-size effects in two respects: on the one hand, for a given volume it yields results that are strongly dependent on the number of vertices in the triple line and still inaccurate for N = 192 (N_v = 7777!); on the other hand, for a given number of vertices the measured average contact angle depends on the volume so that it is slightly decreasing with growing volume of the drop. This means that the results of the direct measurement method depend on the mesh spacing, i.e., the mean edge length in the triangular tessellation of the drop. This dependence can be seen in Figure 4 where we show the results of Figure 3 as a function of the mean edge length in the triple line L/N.

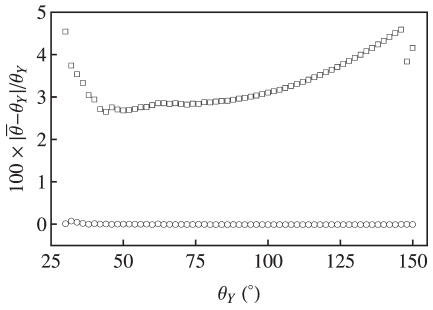

Figure 5. Percent absolute relative deviations of the measured average contact angles from the Young contact angle in a drop of water with V = 0.03 cm^3 and N = 48. Circles: results of the new method based on the measurement of forces. Squares: results of the direct measurement of the contact angles.

To perform a more detailed analysis of the measurement methods, we have considered a drop of water with a fixed volume of V = 0.03 cm^3 with a mesh spacing such that there are N = 48 vertices in the triple line. In the Surface Evolver simulations of this particular system, we have varied the Young contact angle from θ_Y = 30° to 150°, reached equilibrium for each value of θ_Y, and then measured the average contact angle using both methods. In Figure 5, we plot the percent absolute relative deviations of the measured average contact angles from the Young contact angle. For the considered angles, we obtain an average absolute relative deviation of 3.3% for the direct measurement method and of 0.0066% for the new method.

Taking into account the excellent performance of the new method of measuring contact angles, in what follows we shall limit ourselves to this method.

■ COMPARISON WITH DYNAMIC ONE-CYCLE CONTACT ANGLE EXPERIMENTAL DATA

Here we shall compare the results of the preceding Sections with the experimental data of Lam et al.[21] for DOCA measurements of the advancing and receding contact angles of sessile drops.

Figure 6 shows the results for a DOCA experiment for a drop of water on a poly(lactic acid)-coated silicon surface. This case, already considered in Figure 1, provides an excellent example of constant receding contact angle. We compare our theoretical results obtained from the Young−Laplace equation (dashed line) with Surface Evolver simulations (solid line) and experimental data obtained from Figure 3 of ref 21 (symbols). The input data for our calculations are θ_{adv} = 79.82° and θ_{rec} = 60.97°. In addition, we have used the value g = 9.8 m/s^2 for the acceleration of gravity, σ_{lv} = 73 mN/m for the surface tension of water, and ρ = 10^3 kg/m^2 for the density of water. The maximum volume of the drop (0.118 cm^3) and the rate of increase and decrease of the volume are obtained from Figure 6c.

dx.doi.org/10.1021/la202771u |*Langmuir* 2011, 27, 14868–14875

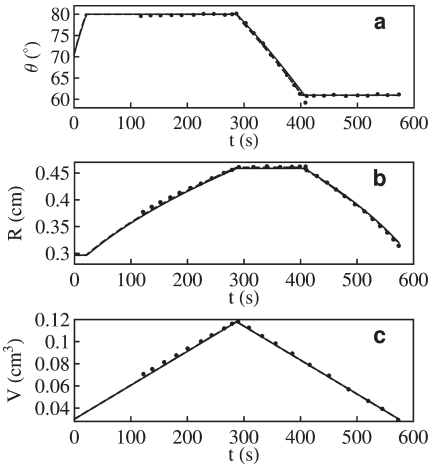

Figure 6. Contact angle hysteresis cycle for a drop of water on a poly(lactic acid)-coated silicon surface. (a) Contact angle θ vs time. (b) Triple-line radius R vs time. (c) Volume V vs time. The solid lines are the results of the Surface Evolver simulations, the dashed lines are theoretical results obtained from the Young−Laplace equation and the symbols are experimental data.[21]

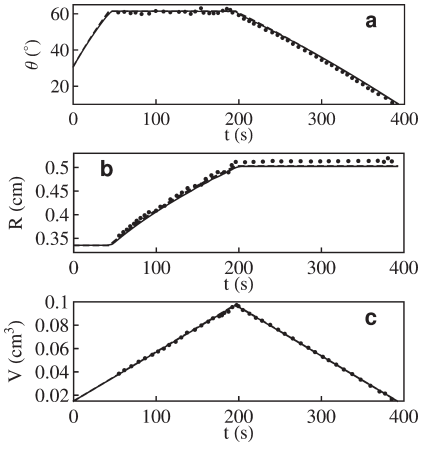

Figure 7. Contact angle hysteresis cycle for formamide on a 50:50 poly(lactic glycolic acid)-coated silicon surface. (a) Contact angle θ vs time. (b) Triple-line radius R vs time. (c) Volume V vs time. The solid lines are the results of the Surface Evolver simulations, the dashed lines are theoretical results obtained from the Young−Laplace equation and the symbols are experimental data.[21]

In Figure 6a, we show the variation with time of the contact angle where we observe an excellent agreement between theory, simulation, and experimental data. We note that the experimental data begin when the system is already in an advancing situation while theory and simulation results have been obtained from a cycle that starts at an initial volume of 0.030 cm^3 with an initial contact angle equal to the Young contact angle which is assumed to take the value $\theta_Y = (\theta_{rec} + \theta_{adv})/2 = 70.40°$. The variation with time of the radius of the triple line is shown in Figure 6b, where theory and simulation show excellent agreement, slightly underestimating experimental data for advancing angles, and slightly overestimating the value of the experimental radius for receding angles.

Figure 7 considers a DOCA experiment for formamide on a 50:50 poly(lactic glycolic acid)-coated silicon surface. In this

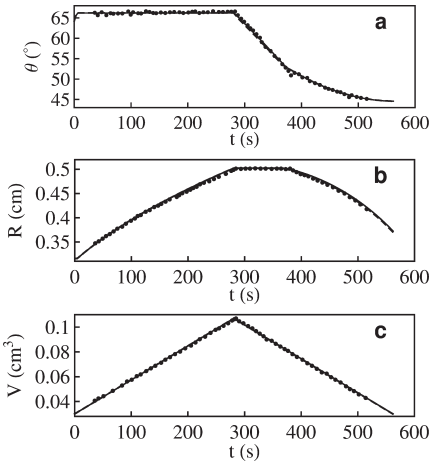

Figure 8. Contact angle hysteresis cycle for formamide on a poly(methyl methacrylate/*n*-butyl methacrylate)-coated silicon surface. (a) Contact angle θ vs time. (b) Triple-line radius R vs time. (c) Volume V vs time. The solid lines are the results of the Surface Evolver simulations, the dashed lines are theoretical results obtained from the Young−Laplace equation and the symbols are experimental data.[21]

case, the receding contact angle is absent. The experimental data have been obtained from Figure 5 of ref 21. The input data for our calculations are $\theta_{adv} = 61.5°$ and $\theta_{rec} = 0°$. We have used the value $\rho = 1.13 \times 10^3$ kg/m^2 for the density of formamide and we have considered $\sigma_{lv} = 52.5$ mN/m for the surface tension of formamide in order to be consistent with the results for σ_{lv} shown in Figure 5 of ref 21. Theory and simulation results have been obtained from a cycle that starts at an initial volume of 0.015 cm^3 with an initial contact angle equal to 30.75°. Like in the preceding case, the maximum volume 0.0975 cm^3 and its rate of variation have been obtained from the experimental data of Figure 7c. In this case, theory and simulation present excellent agreement both for the contact angles and for the triple-line radius but comparison with experimental data yields a slightly worse agreement than in the case of Figure 6, underestimating the radius of the triple line for receding contact angles.

Figure 8 presents a situation with a time-dependent receding contact angle that arises for formamide on a poly(methyl methacrylate/*n*-butyl methacrylate)-coated silicon surface. The experimental data have been obtained from Figure 2 of ref 21. As previously mentioned, most liquid−solid systems give rise to time-dependent receding contact angles due to surface swelling and adsorption. Since a microscopic approach to this situation is beyond the scope of this work, we follow Lam et al.[21] by considering a quadratic least-squares fit to the time-dependent receding contact angles (from $t \approx 390$ s). We obtain the following:

$$\theta_{rec}(t) = 117.325 - 0.25833t + 0.0002935t^2 \qquad (25)$$

Extrapolating to the time where the volume starts to decrease, we obtain the initial receding contact angle $\theta_{rec,ini} = \theta_{rec}(285) \approx 62.3°$. This initial receding contact angle is expected to be the receding contact angle before any solid−liquid interaction takes place.[21] From the experimental data of Figure 8, we obtain $\theta_{adv} = 66.2°$. For the sake of consistency with the results for σ_{lv} shown in Figure 2 of ref 21, in this particular case, we have considered a value of 54.5 mN/m for the surface tension of formamide.

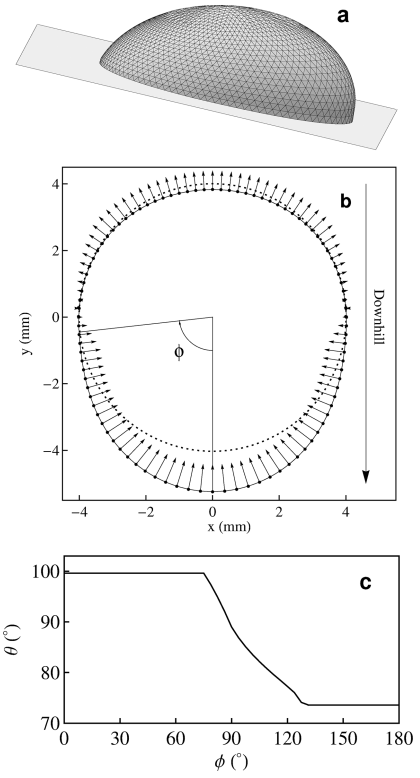

Figure 9. Surface Evolver results for a drop in a tilted plane ($\alpha = 13°$). (a) The shape of the drop. (b) Triple contact line showing the position of the vertices and the friction forces acting on them (see text). The dotted line represents the contact line for the initial, untilted situation ($\alpha = 0°$). (c) Contact angles as a function of the angle ϕ defined in (b).

Theory and simulation results in Figure 8 have been obtained from a cycle that starts at an initial volume of 0.03 cm^3 and reaches a maximum volume of 0.107 cm^3. The initial contact angle has been taken equal to $(\theta_{rec,ini} + \theta_{adv})/2 = 64.25°$. Of course, instead of using a constant receding contact angle, in this case, for decreasing volumes we have considered the time-dependent receding contact angle of eq 25. Like in the previous case, theory and simulation present excellent agreement both for the contact angles and for the triple-line radius. Comparison with experimental data also gives very good agreement for the contact angles while the triple-line radius is slightly overestimated.

RESULTS FOR LIQUID DROPS ON INCLINED PLANES

Until now, we have restricted ourselves to axisymmetric drops that can be studied both theoretically and with Surface Evolver simulations. Here, we shall present our results for drops on inclined planes. In this case, the shape of the drop is no longer axisymmetric and therefore we shall only consider Surface Evolver simulations.

In Figure 9, we present our simulation results for a drop of water of volume $V = 0.116$ cm^3 on an inclined PCTFE surface. We have considered $\theta_{adv} = 99.6°$ and $\theta_{rec} = 73.6°$ which are the critical advancing and receding contact angles obtained by Extrand and Kumagai[37] for water on an inclined PCTFE surface. In our simulations, we have considered a tilt angle $\alpha = 13°$, which is close to the critical tilt for the volume considered. In order to mimic the experiments, we have started with an untilted surface in which a drop of water has been made grow until the desired volume is obtained. This leads to the fact that the initial contact angle of the drop is the advancing angle. Then the plane is slowly tilted, reaching equilibrium for each intermediate tilt angle, up to the final tilt angle. Measurements are made after a long equilibration period.

Figure 9a shows the stable shape of the drop as obtained in the Surface Evolver using our gfric command instead of g. As one can observe, the drop is no longer axisymmetric due to the balance between gravity forces in an inclined surface and the retentive forces due to contact angle hysteresis. Figure 9b shows the triple contact line, also showing the position of the vertices and the retentive forces F_i/σ_{lv} acting on them. For clarity, we have scaled F_i/σ_{lv} by a factor of 10 so that their units are 10^{-1} mm instead of mm. We note that these forces balance in the "X" axis and lead to a net retentive force in the "Y" axis of the inclined plane. This net retentive force balances the effect of gravity. In order to show the deformation of the contact line due to the tilting we also plot with dots the triple contact line for the initial untilted situation with $\alpha = 0°$. Figure 9c shows the contact angles as a function of the angle ϕ defined in Figure 9b. We note that at the front of the drop the contact angles are equal to $\theta_{adv} = 99.6°$, while at the rear, the contact angles are equal to $\theta_{rec} = 73.6°$.

CONCLUSIONS

In this work, we have proposed a simple model for dealing with the contact angle hysteresis of drops on a planar surface. Inspired by the pioneering work of Adam and Jessop,[6] we have included a friction force per unit length in Young's equation, allowing us to establish a relationship between contact angles and friction forces and to obtain the maximum advancing and receding forces. The friction force acts on the triple line so that it remains fixed for contact angles in the interval $\theta_{rec} \leq \theta \leq \theta_{adv}$.

On the basis of the solution of the Young−Laplace equation for cylindrical symmetry, the model has been applied to axisymmetric drops with remarkable agreement with the results of the DOCA experiments. The model has also been implemented in the Surface Evolver, where it can be used both for axisymmetric and nonaxisymmetric drops. In addition, given the relation between contact angles and friction forces, by measuring the forces acting on the triple line one is provided with a new way of measuring contact angles in the Surface Evolver, which has been shown to be more accurate than the direct measurement of contact angles.

The Surface Evolver results for axisymmetric drops yield excellent agreement with data obtained in DOCA experiments, even for situations with time-dependent receding contact angles, although in this case one must resort to a fitting function for the receding contact angles, instead of using a constant receding contact angle as an input.

We have presented also a few results for nonaxisymmetric drops in an inclined surface. A complete analysis of this situation is in progress and will be the subject of a forthcoming publication.

AUTHOR INFORMATION

Corresponding Author
*E-mail: white@usal.es.

Present Addresses
‡Also at IUFFyM, Universidad de Salamanca, Spain.

■ ACKNOWLEDGMENT

We would like to thank F.L. Román for a careful reading and commenting on the manuscript. We are thankful for financial support from the Ministerio de Educación y Ciencia of Spain under Grant FIS2009-07557.

■ REFERENCES

(1) Young, T. *Philos. Trans. R. Soc. London* **1805**, *95*, 65–87.
(2) Marmur, A. *Soft Matter* **2006**, *2*, 12–17.
(3) Cassie, A. B. D. *Discuss. Faraday Soc.* **1948**, *3*, 11–16.
(4) Wenzel, R. *Ind. Eng. Chem.* **1936**, *28*, 988–994.
(5) Cassie, A. B. D.; Baxter, S. *Trans. Faraday Soc.* **1944**, *40*, 546–551.
(6) Adam, N. K.; Jessop, G. *J. Chem. Soc., Trans.* **1925**, *127*, 1863.
(7) Good, R. J. *J. Am. Chem. Soc.* **1952**, *74*, 5041–5042.
(8) Wolfram, E.; Faust, R. In *Wetting, Spreading and Adhesion*; Padday, J. F., Ed.; Academic Press: London, 1978; Chapter "Liquid Drops on a Tilted Plate, Contact Angle Hysteresis and the Young Contact Angle", pp 213−222.
(9) Brown, R. A.; Orr, F. M.; Scriven, L. E. *J. Colloid Interface Sci.* **1980**, *73*, 76–87.
(10) Milinazzo, F.; Shinbrot, M. *J. Colloid Interface Sci.* **1988**, *121*, 254–264.
(11) Dussan, E.; Chow, R. *J. Fluid Mech.* **1983**, *137*, 1–29.
(12) Dussan, V. *J. Fluid Mech.* **1985**, *151*, 1–20.
(13) Iliev, S. D. *Comput. Methods Appl. Mech. Eng.* **1995**, *126*, 251–265.
(14) Iliev, S. D. *J. Colloid Interface Sci.* **1997**, *194*, 287–300.
(15) Dimitrakopoulos, P.; Higdon, J. *J. Fluid Mech.* **1999**, *395*, 181–209.
(16) Joanny, J. F.; de Gennes, P. G. *J. Chem. Phys.* **1984**, *81*, 552–562.
(17) de Gennes, P. G. *Rev. Mod. Phys.* **1985**, *57*, 827–863.
(18) Brakke, K. *Exp. Math.* **1992**, *1*, 141–165.
(19) Laplace, P. S. *Traité de Mécanique Céleste*; Gauthier-Villars: Paris, 1806; Vol. 4, Supplement to Book 10; p 419.
(20) del Río, O. I.; Neumann, A. W. *J. Colloid Interface Sci.* **1997**, *196*, 136–147.
(21) Lam, C. N. C.; Wu, R.; Li, D.; Hair, M. L.; Neumann, A. W. *Adv. Colloid Interface Sci.* **2002**, *96*, 169–191.
(22) Vargha-Butler, E. I.; Kiss, E.; Lam, C. N. C.; Keresztes, Z.; Kálmán, E.; Zhang, L.; Neumann, A. W. *Colloid Polym. Sci.* **2001**, *279*, 1160–1168, DOI: 10.1007/s003960100549.
(23) Tadmor, R. *Langmuir* **2004**, *20*, 7659–7664.
(24) Brandon, S.; Wachs, A.; Marmur, A. *J. Colloid Interface Sci.* **1997**, *191*, 110–116.
(25) Patankar, N.; Chen, Y. Numerical simulation of droplet shapes on rough surfaces. 2002.
(26) Berthier, J.; Clementz, P.; Raccurt, O.; Jary, D.; Claustre, P.; Peponnet, C.; Fouillet, Y. *Sens. Actuators A: Phys.* **2006**, *127*, 283−294, MEMS 2005 Special Issue - Special Issue of the Micromechanics Section of Sensors and Actuators (SAMM), based on contributions revised from the technical digest of the IEEE 18th International Conference on Micro Electro Mechanical Systems (MEMS-2005).
(27) Berthier, J. *Microdrops and Digital Microfluidics: Processing, Development, and Applications*; William Andrew Publishing: Burlington, MA, 2007.
(28) Berthier, J.; Dubois, P.; Clementz, P.; Claustre, P.; Peponnet, C.; Fouillet, Y. *Sens. Actuators A: Phys.* **2007**, *134*, 471–479.
(29) Monnereau, C.; Pittet, N.; Weaire, D. *Europhys. Lett.* **2000**, *52*, 361–367.
(30) Rayner, M.; Trägårdh, G.; Trägårdh, C.; Dejmek, P. *J. Colloid Interface Sci.* **2004**, *279*, 175–185.
(31) Cox, S. *Colloids Surf., A* **2005**, *263*, 81–89A collection of papers presented at the 5th European Conference on Foams, Emulsions, and Applications, EUFOAM 2004, University of Marne-la-Vallee, Champs sur Marne (France), 5−8 July, 2004.
(32) Lienemann, J.; Greiner, A.; Korvink, J. *IEEE Trans. Comput.-Aided Des. Integ. Circ. Syst.* **2006**, *25*, 234–247.
(33) Dorrer, C.; Rühe, J. *Langmuir* **2007**, *23*, 3179–3183.
(34) Dorrer, C.; Rühe, J. *Langmuir* **2007**, *23*, 3820–3824.
(35) Dorrer, C.; Rühe, J. *Langmuir* **2008**, *24*, 1959−1964, PMID: 18217779.
(36) Forsberg, P. S. H.; Priest, C.; Brinkmann, M.; Sedev, R.; Ralston, J. *Langmuir* **2010**, *26*, 860−865, PMID: 19702258.
(37) Extrand, C. W.; Kumagai, Y. *J. Colloid Interface Sci.* **1995**, *170*, 515–521.